12-2016

A laboratory facility to study gas-aerosol-cloud interactions in a turbulent environment: The Π Chamber

K. Chang
Michigan Technological University

J. Bench
Russells Technical Products

M. Brege
Michigan Technological University

Will Cantrell
Michigan Technological University

K. Chandrakar
Michigan Technological University

See next page for additional authors

Recommended Citation

Chang, K., Bench, J., Brege, M., Cantrell, W., Chandrakar, K., Ciochetto, D., Mazzoleni, C., Mazzoleni, L., Niedermeier, D., & Shaw, R. A. (2016). A laboratory facility to study gas-aerosol-cloud interactions in a turbulent environment: The Π Chamber. *Bulletin of the American Meteorological Society, 97*(12), 2343-2358. http://doi.org/10.1175/BAMS-D-15-00203.1
Retrieved from: https://digitalcommons.mtu.edu/physics-fp/97

Follow this and additional works at: https://digitalcommons.mtu.edu/physics-fp

 Part of the Atmospheric Sciences Commons, and the Physics Commons

A LABORATORY FACILITY TO STUDY GAS–AEROSOL–CLOUD INTERACTIONS IN A TURBULENT ENVIRONMENT

The Π Chamber

BY K. CHANG, J. BENCH, M. BREGE, W. CANTRELL, K. CHANDRAKAR, D. CIOCHETTO, C. MAZZOLENI, L. R. MAZZOLENI, D. NIEDERMEIER, AND R. A. SHAW

A turbulent, multiphase reaction chamber has been developed that is capable of generating and sustaining cloud formation in simulated tropospheric conditions for minutes to days.

To understand Earth's climate system, the interactions among aerosols, cloud droplets, ice crystals, and trace gases within the turbulent atmosphere must be known (e.g., Feingold and Siebert 2009). Extensive research activity during the last decades has yielded significant progress, but many of these interactions are still poorly understood and ill quantified (e.g., Quaas et al. 2009). For example, every cloud droplet in Earth's atmosphere (~10^{25}) was catalyzed by a preexisting aerosol particle, but not every aerosol particle becomes a cloud droplet. The particle-to-droplet transformation, known as activation, requires that the particle be exposed to some critical concentration of water vapor, which varies for different combinations of particle size and chemical composition. Similarly, the formation of ice particles in the atmosphere is often catalyzed by aerosol particles, either activated or not (Cantrell and Heymsfield 2005). Even in the simplest scenarios, it is challenging to gain a full understanding of the aerosol activation and ice nucleation processes, but at least two other factors contribute greatly to the complexity observed in the atmosphere. First, aerosols and cloud particles are not static entities but are continuously interacting with their chemical environment and therefore changing in their properties. Second, clouds are ubiquitously turbulent, and therefore thermodynamic and compositional variables, such as ▶

water vapor or trace gas concentrations, fluctuate in space and time. Indeed, the coupling between turbulence and microphysical processes is recognized as one of the major research challenges in cloud–aerosol physics today (Bodenschatz et al. 2010). These aerosol–cloud transformations and the chemical and turbulent processes that influence them are the scientific context of this article.

We have developed an interdisciplinary research facility for laboratory investigation of physical and chemical processes occurring in atmospheric aerosols and clouds under well-characterized turbulent conditions. Within the U.S. atmospheric sciences community there has been a sense that laboratory research in aerosol and cloud science has lagged progress in computational and field-based efforts (List et al. 1986; National Research Council 2003; Fremaux and Bushnell 2011), but it is also widely recognized that new capabilities and instrumentation have opened up greater possibilities (e.g., Ghan and Schwartz 2007; Stratmann et al. 2009). A well-designed laboratory system is not aimed at simulating the full complexity of cloud processes but rather is a purposeful attempt at providing an idealized, controlled environment in which specific mechanisms can be investigated with repeatability and with known initial and boundary conditions. That simplification puts laboratory experiments at the very foundation of the discipline, as captured in this recommendation for improvement of model treatment of cloud and precipitation physics in a recent National Research Council report (National Research Council 2003, p. 7): "Such studies must be based on cloud physics laboratory measurements, tested and tuned in model studies, and validated by in situ and ground observations." With this chamber we are able to address at the fundamental level many of the processes interconnecting clouds (both liquid water and ice), aerosols, water vapor, trace gases, thermodynamics, and turbulence.

Over the last few decades a number of aerosol–cloud chambers have been used for scientific research of relevance to the atmospheric sciences. We summarize some of the most well-known chambers in Table 1, including their basic operating principles, typical research applications, and a representative paper for further details. There also exists a wide range of other laboratory facilities for aerosol and cloud research, such as continuous flow systems (Stratmann et al. 2004; Stetzer et al. 2008), wind tunnels (List et al. 1987; Beard and Pruppacher 1969), turbulence chambers (Lu et al. 2010; Bewley et al. 2013), and electrodynamic balances (Duft and Leisner 2004; Rzesanke et al. 2012). These and other laboratory chambers and facilities have been essential in filling gaps in the big puzzle of understanding aerosol–cloud interactions. But, as already mentioned above, key aspects, connections, and details remain unresolved. The turbulent aerosol–cloud reaction chamber, which we call the Π chamber because of its working volume of 3.14 m^3 (with the cylindrical insertion in place; see Fig. 1 and text below), is intended to play a part in filling these gaps. We are able to study cloud microphysics and turbulence coupling within a thermodynamically controlled environment, making this chamber unique compared to many of the above-mentioned chambers/facilities. Steady-state cloud conditions can be achieved on time scales of hours to days, enabling measurements where long time averaging is helpful, including turbulence studies, nucleation experiments, and instrument calibration. The ability to study phase and chemical transformations and partitioning in a well-characterized turbulent environment is unique among the existing laboratory facilities within the United States.

The turbulent aerosol–cloud reaction chamber can serve as a research focal point, enabling scientists with broad-ranging interests to address interdisciplinary problems. We anticipate that the chamber will serve as a facility capable of attracting researchers from throughout the United States and the international atmospheric sciences community. The research problems that can be addressed with this facility range from aerosol formation and optical properties to turbulence and ice nucleation. In what follows, the chamber and accompanying instrumentation is described in the section titled "Technical description of the chamber," followed by a description of the two primary cloud formation mechanisms in the

AFFILIATIONS: Chang, Cantrell, Chandrakar, Ciochetto, C. Mazzoleni, Niedermeier,* and Shaw—Department of Physics, and Atmospheric Sciences Program, Michigan Technological University, Houghton, Michigan; Bench—Russells Technical Products, Holland, Michigan; Brege and L. Mazzoleni—Department of Chemistry and Atmospheric Sciences Program, Michigan Technological University, Houghton, Michigan
***CURRENT AFFILIATION:** Leibniz Institute for Tropospheric Research, Leipzig, Germany
CORRESPONDING AUTHOR: R. A. Shaw, Dept. of Physics, Michigan Technological University, 1400 Townsend Drive, Houghton, MI 49931
E-mail: rashaw@mtu.edu

The abstract for this article can be found in this issue, following the table of contents.
DOI:10.1175/BAMS-D-15-00203.1

In final form 15 March 2016

chamber in the section titled "Cloud formation in the chamber." Finally, in the section titled "Results from preliminary experiments," we outline a few preliminary results from the chamber and discuss its potential for addressing current problems in cloud–aerosol physics and chemistry.

Table 1. A representative list of cloud chambers that have been focused on cloud and aerosol research.

Name	Type	Reference	Location	Operational since	Studies
Aerosol Interaction and Dynamics in the Atmosphere (AIDA) chamber	Expansion-type cloud chamber	Möhler et al. (2003)	Karlsruhe, Germany	1996–present	Aerosol and cloud chemistry, cloud microphysics (especially ice nucleation studies), aerosol and cloud radiative properties
Calspan chamber	Expansion-type cloud chamber	Hoppel et al. (1994)	Ashford, New York	1980s–present	Aerosol and cloud chemistry, cloud microphysics, aerosol and cloud radiative properties
Experimental Multiphasic Atmospheric Simulation Chamber (CESAM)	Multiphase reaction chamber	Wang et al. (2011)	Créteil, France	~2009–present	Aerosol and cloud photochemistry
Colorado State University (CSU) chamber	Adiabatic expansion-type cloud chamber	DeMott and Rogers (1990)	Fort Collins, Colorado	Out of operation	Cloud microphysics (especially ice nucleation studies)
Cosmics Leaving Outdoor Droplets (CLOUD) chamber	Multiphase reaction chamber	Duplissy et al. (2010)	European Organization for Nuclear Research (CERN), France/ Switzerland	2006–present	Influence of galactic cosmic rays on particle formation and aerosol chemistry, cloud chemistry and microphysics
Desert Research Institute (DRI) chamber	Adiabatic expansion-type cloud chamber	Stehle et al. (1981)	Reno, Nevada	Out of operation	Cloud chemistry
Energy Research Centre of the Netherlands (ECN) high-flow cloud chamber	Turbulent cloud wind tunnel	Khlystou et al. (1996)	Petten, the Netherlands	1996–present	Aerosol–cloud interactions
Manchester Ice Cloud Chamber (MICC)	Fall tube	Connolly et al. (2012)	Manchester, United Kingdom	2009–present	Cloud microphysics (e.g., ice nucleation and aggregation), cloud radiative properties, and thunderstorm electrification
Meteorological Research Institute (MRI) chamber	Adiabatic expansion-type cloud chamber	Tajiri et al. (2013)	Tsukuba, Japan	2012–present	Cloud microphysics (cloud droplet/ice crystal formation and growth), aerosol scavenging
Penn State University chamber	Mixing chamber	Song and Lamb (1994)	University Park, Pennsylvania	Out of operation	Cloud chemistry and microphysics
University of Manchester Institute of Science and Technology (UMIST) chamber	Fall tube	Latham and Reed (1977)	Manchester, United Kingdom	Out of operation	Cloud mixing processes
University of Missouri–Rolla (UMR) chamber	Adiabatic expansion-type cloud chamber	Hagen et al. (1989)	Rolla, Missouri	Out of operation	Cloud microphysics

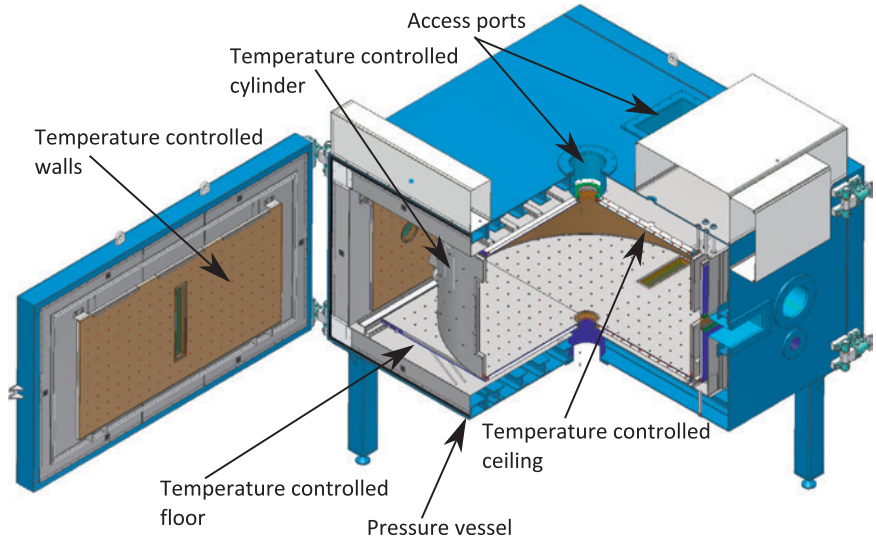

Fig. 1. A cutaway schematic of the cloud chamber with one door open and the cylindrical thermal panel in place.

TECHNICAL DESCRIPTION OF THE CHAMBER. The Π chamber is designed to provide an environment matching typical cloud conditions in Earth's troposphere. It can achieve pressures ranging from 60 hPa to "surface" values of 1,000 hPa and can sustain temperatures of –55° to 55°C, thereby allowing for investigation of both warm and cold (including mixed phase) cloud processes. The chamber can be operated in expansion, static diffusion, or turbulent mode, depending on the requirements of a particular experiment (further explanation and details are given in the section titled "Cloud formation in the chamber").

As shown in Fig. 1, the pressure shell is rectangular. The internal volume available for experiments is 5 m^3; this volume is reduced to 3.14 m^3 when the cylindrical thermal panel (1 m high, 2-m diameter) is installed. The pressure shell is constructed from welded steel plates, which are reinforced to withstand the pressure differential when the internal pressure is reduced below atmospheric pressure. A layer of foam glass, 20 cm in thickness, between the outer pressure shell and the inner, electro-polished stainless steel lining provides insulation from the surrounding environment. Two front-opening hinged doors give full access to the internal workspace. A fisheye lens photo of the cloud chamber laboratory is shown in Fig. 2.

The heat transfer system connecting the reservoir in the control section and the thermal panels, which are in direct contact with the air inside the chamber, is a closed-loop system containing Dynalene HF-LO heat transfer fluid (Dynalene, Inc., Whitehall, Pennsylvania). The Dynalene is cooled to 2° (controllable) below the minimum temperature in the chamber and then heated to the desired temperature of each zone within the chamber, using an electric element for each one. The heaters are staged for ease of regulating the thermal input for varying load and temperature conditions.

The thermal panels, which regulate the temperature within the chamber, are controlled on three separate circuits, corresponding to the top, bottom, and sidewall sections of the chamber internal workspace. The heat transfer fluid is introduced to the panels through copper tubing that is snaked through the volume of the panel. The tubing is drilled such that the fluid escapes from it and into the panel's interior volume uniformly, which minimizes temperature gradients across them. In some circumstances, such as when idealized Rayleigh–Bénard convection is desired, we reduce heat transfer from the walls by covering them with 3.2-mm-thick polycarbonate sheets. A cylindrical stainless steel thermal panel (of the same design as those just described and with dimensions given above) provides an alternative to the rectangular geometry. For Rayleigh–Bénard convection with wet top and bottom boundaries, glass fiber filter paper (type A/E glass fiber, Pall Corporation, Dreieich, Germany) covers the top and bottom panels and can be connected to water reservoirs to ensure long lifetime liquid (or ice) boundaries.

As shown schematically in Fig. 1, the chamber has various pairs of oppositely positioned access ports. There are several 25- and 10-cm flanges for electrical, mechanical, and optical access. For experiments that demand a larger access area, there are also larger rectangular ports available: two aligned vertically and two horizontally. There are also two rectangular and two circular windows placed on the top and bottom surfaces.

The chamber has been programmed with manufacturer preset safety limits to protect the system from exceeding design limits. The pressure shell has a pressure relief valve that limits the operational pressure to atmospheric conditions. We use only true linear pressure transducers for pressure control. The machine unit containing the heat exchanger, the

pump, and the cascade refrigeration system is isolated from the chamber in a separate housing. To reduce noise produced by the unit, a layer of 2.5-cm-thick foam coats the entire housing.

The temperatures and pressure used as input to the chamber's proportional-integral-derivative (PID) controls are monitored and displayed with a temporal resolution of 1 Hz. A snapshot of that data, along with diagnostic data from the machine section, is recorded every minute. For higher-resolution data, used to investigate turbulence, for example, there are dedicated instruments with separate data acquisition. The chamber is also accompanied by a suite of instrumentation allowing for the generation and characterization of aerosol and cloud particles, measurement of thermodynamic and turbulence conditions, and sampling of particles for subsequent chemical and morphological analysis. Table 2 is the list of instruments currently associated with the chamber.

CLOUD FORMATION IN THE CHAMBER. The combination of all physical variables accessible with the Π chamber is enormous. Therefore, we highlight a few prominent features and streamline our presentation as follows. First, we demonstrate the intrinsic response of the chamber to arbitrarily imposed pressure and temperature conditions. Thereafter, in the sections titled "Expansion cloud" and "Steady-state turbulent mixing cloud," we discuss data from the two primary cloud formation mechanisms possible with the chamber.

The left panel of Fig. 3 shows the maximum rate of response of the pressure during an expansion within

Fig. 2. Photograph of the cloud chamber with scientists for scale. Photo credit: S. Bird, Michigan Technological University.

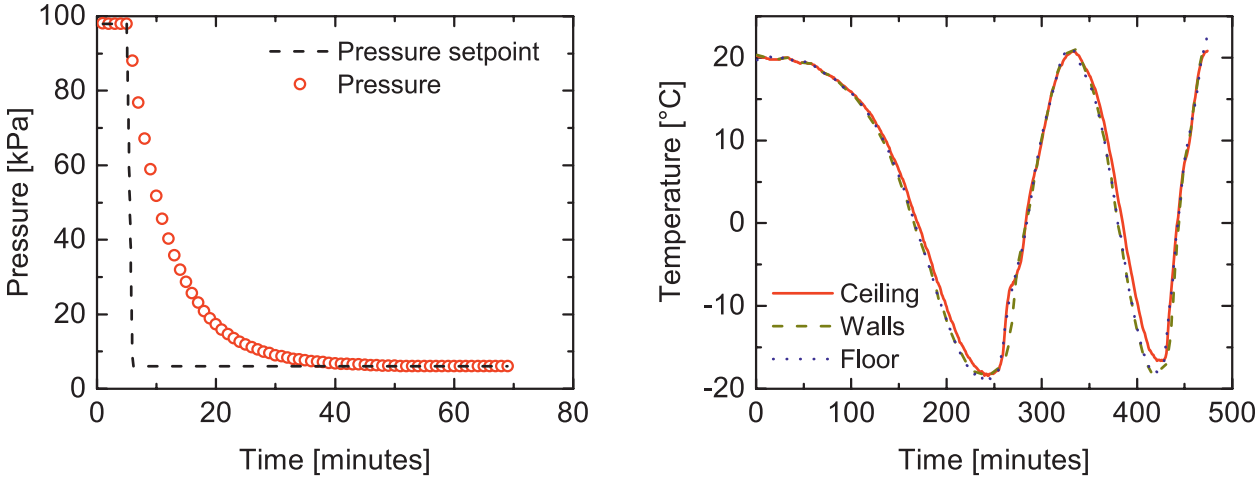

Fig. 3. Examples of the pressure and temperature response in the Π chamber.

the chamber. By fitting an exponential of the form $p_0 e^{-t/\tau_p}$ to the part of the curve that corresponds to the expansion, we estimate the relaxation time τ_p to be approximately 7.5 min, which yields a maximum expansion rate of about –220 Pa s^{-1}. The pumping rate can be precisely controlled at lower values via the PID system.

As noted in the section titled "Technical description of the chamber," the temperature of the three zones within the chamber can be controlled independently. To illustrate the ability to control the three heating zones, the right panel of Fig. 3 shows the response of the surface of the radiant panels to an isothermal temperature "chirp." The maximum possible rate of change is approximately 1 K min^{-1}. Varying the temperature as a function of time can be used to track the temperature of the interior surfaces in order to mitigate wall effects due to mixing within the chamber, thereby making the expansion as adiabatic as possible.

Expansion cloud. The classical Aitken dust counter (Aitken 1889) and its cousin, the Wilson chamber (Wilson 1911), have played an important role in atmospheric research for over 100 years. In both instruments, the enclosed mixture of air and water vapor is adiabatically expanded to locally reduce the air temperature, thereby generating supersaturated conditions and inducing water vapor to form cloud droplets on any cloud condensation nuclei (CCN) present in the air. Most modern cloud chambers have also employed this method for cloud generation

Table 2. List of instrumentation currently available for use with the chamber.

Instrument	Function
TSI atomizer (3076)	Generation of soluble aerosol particles, for example, NaCl or ammonium sulfate
TSI fluidized bed (3400A)	Dispersal of dry aerosol particles such as mineral dust
PALAS condensation particle generator (MAG 3000)	Generation of nearly monodisperse semivolatile aerosols
TSI differential mobility analyzer (DMA, 3080L)	Size selection of aerosol particles up to 1 μm
TSI scanning mobility particle sizer [DMA+CPC (3772)]	Measurement of the aerosol size distribution from 10 nm to 1 μm
TSI optical particle sizer (OPS, 3330)	Measurement of the aerosol size distribution from 0.3 to 10 μm
Photoacoustic nephelometer spectrometer (custom)	Measurement of absorption and scattering of aerosol at three wavelengths
DMT SP2 soot photometer	Detection of aerosol particles through their scattering signal and quantification of the soot content through incandescence
Cambustion centrifugal particle mass analyzer	Size selection of aerosol based on mass to charge ratio, can be used to provide information on the shape of particles when coupled with the DMA
Brechtel Mfg. pumped counter flow virtual impactor (CVI)	Separation of cloud droplets and/or crystals from interstitial aerosol
DMT cloud condensation nucleus counter (CCN-100)	Measurement of the cloud condensation nucleus spectrum
Applikon analytical PILS (ADI 2081)	Collection by impaction of aerosol and cloud particles into solution for subsequent chemical analysis
Dantec phase Doppler interferometer (Flow Explorer, HiDense Fiber detector, and Burst Spectrum Analyzer)	Measurement of the cloud droplet size distribution and two components of the droplet velocity vector
Holographic cloud measurement system (custom)	Measurements of the cloud droplet and ice crystal size distribution along with three-dimensional positions of the hydrometeors
LI-COR LI-7500A open path H_2O analyzer	Measurement of the water vapor concentration in the chamber with a frequency up to 20 Hz
Lakeshore 218 temperature monitor and resistance thermometers (Minco)	Measurement of temperature in the chamber
Applied Technologies, Inc., sonic anemometer–V probe	Measurement of the air velocity vector with a frequency up to 20 Hz and an integration path of 10 cm
2D cloud imaging system (custom)	Spatial and temporal distribution of cloud with a laser light sheet and camera
Thermistor array	Measurement of temperature spatial profile in the chamber

(see, e.g., Möhler et al. 2003). The expansion occurs naturally in the atmosphere in the form of large-scale ascent during free convection. If the rate of ascent is rapid compared to diffusion or mixing processes, the temperature of the air in the parcel (prior to saturation) can be approximated by the adiabatic value, given by $T_{ad} = T_{ref}(p/p_{ref})^{R/c_p}$, where T_{ref} and p_{ref} are the pressure and temperature at some reference value, usually the values corresponding to the level at which the ascent started, and R and c_p are the gas constant and specific heat at constant pressure of the gas in question (Wallace and Hobbs 1977). After saturation, the lapse rate is modified because of the enthalpy of vaporization of water as cloud formation occurs. Cloud chambers operating in expansion mode mimic this natural process, although the presence of walls inevitably limits the time under which adiabatic conditions can be maintained.

Data from a representative expansion in the Π chamber are shown in Fig. 4. Starting from site level pressure of approximately one atmosphere, the pressure was reduced to 500 hPa in 7 min. The temperatures as measured in six places by resistance thermometers fastened to a line running diagonally from one of the lower corners (T1) to the opposite, upper corner (T6) show that the temperature decreases initially as the pressure is reduced but reaches a minimum and starts to increase as heat from the walls and pressure shell mixes into the interior of the chamber. The mixing is also evident from a comparison of the measured temperature with the adiabatic temperature of –33°C upon reaching 500 hPa; the discrepancy of over 40 K shows that the range of cooling that we can achieve through adiabatic expansion is limited by mixing processes. The situation can be improved by ramping the temperature of the control surfaces downward at the rate expected from the adiabatic expansion. In those cases, we pump much more slowly as the maximum rate of cooling of the surfaces is approximately 1 K min^{-1}. The dramatic increase in temperature evident in the figure is the result of adiabatic compression of the gas as pressure is increased to site level again.

Prior to an expansion cloud experiment, the chamber is typically pumped to less than 100 hPa and repressurized with clean, dry air four to five times to reduce the residual aerosol concentration in the chamber to 10 cm^{-3} or less. The aerosol particles of interest are then injected into the chamber. In the case shown here, we use a constant output atomizer (see Table 2) with a 0.1 g L^{-1} concentration of NaCl. Representative number distributions of aerosol particles in the chamber before expansion are shown in black in the upper panel of Fig. 5; distributions acquired after the cloud cycle and subsequent repressurization are shown in red. A cloud droplet number distribution from the expansion is shown in the lower panel of Fig. 5. The number concentration of cloud droplets during the expansion, as measured with the phase Doppler interferometer (PDI), was 3,240 ± 50 cm^{-3}. We can estimate the maximum supersaturation in the chamber by integrating the aerosol distributions acquired before expansion from the maximum size measured to smaller sizes until the cloud droplet number is reached. [Recall that smaller particles require higher supersaturations

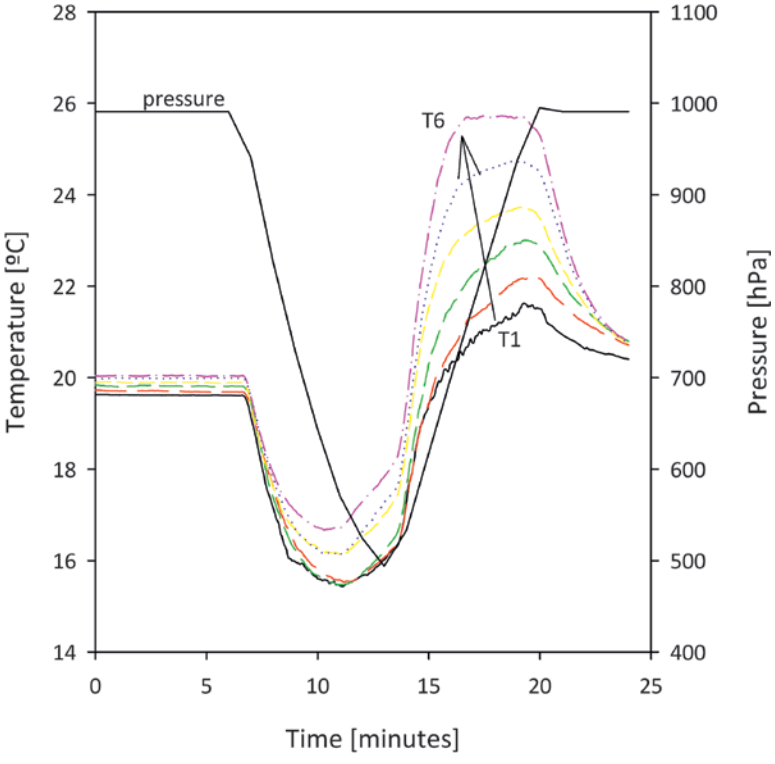

Fig. 4. Pressure (right axis) and temperature (left axis) measured in the chamber as a function of time during an expansion. Temperatures are measured at six (T1–T6) points in the chamber. The pressure is recorded every minute while the temperature is recorded at 1 Hz. Pressure data were interpolated to the higher frequency for the purposes of data visualization and analysis.

for activation (Lamb and Verlinde 2011, chapter 3).] The cloud droplet number concentration is equal to the number concentration of aerosol particles between 36 and 289 nm, indicating that the maximum supersaturation reached during the expansion was 0.56%, using the fact that all particles were NaCl and converting particle diameter to a critical supersaturation using κ-Köhler theory (Petters and Kreidenweis 2007). The fact that 36 nm is well within the minimum seen in the distributions measured after repressurization is suggestive of a process in which some aerosol particles became cloud droplets while smaller ones did not.

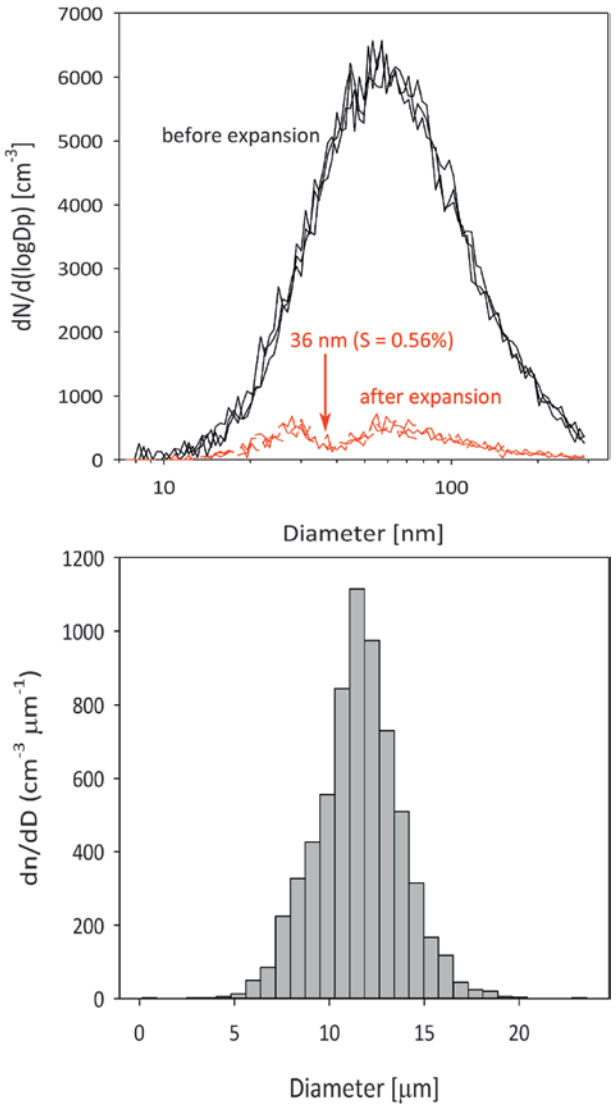

Fig. 5. (top) Aerosol number distributions from the chamber before and after forming an expansion cloud. (bottom) Cloud droplet number distribution from the expansion cloud formed on the aerosol particles shown in the top panel.

Finally, comparison of aerosol number distributions before and after expansion provides an indication of the losses of cloud droplets in the chamber. The initial aerosol number of 4,030 cm^{-3} is reduced to 350 cm^{-3} upon repressurization. Dilution would only have reduced the concentration to 2,015 cm^{-3}; the remaining aerosol must have been scavenged from the chamber as cloud droplets were removed through sedimentation or collisions with the walls. Note, for example, in the lower panel of Fig. 5 that there are already droplets with diameters of 20 μm, a size that will fall out through the chamber's 1-m height in about 1 min. Scavenging losses of aerosols to the walls are also a factor because of the high surface to volume ratio of the chamber.

Steady-state turbulent mixing cloud. The second method of cloud formation possible in the chamber is through creation of a mixing cloud by forcing a negative temperature gradient between the top and bottom surfaces within the chamber. In that case, warm, saturated air originating at the bottom surface mixes with cold, saturated air originating at the top surface. The resulting cloud in the chamber is analogous to walking outside and exhaling on a cold day.

The LI-COR H_2O analyzer and sonic anemometer, as well as eight resistance thermometers (RTDs) were used to characterize the turbulent air motion and thermodynamic variables in the chamber. NaCl aerosol particles were created with an atomizer and the resulting stream of aerosol-laden air was diluted with particle-free air to reach the desired concentration. Cloud droplet sizes and motions were recorded with the phase Doppler interferometer; a vertically oriented laser sheet was also shining through the chamber in order to visualize the motion of the cloud droplets (see http://digitalcommons.mtu.edu/physics-fp/11/ for a video of a cloud in the chamber.)

The measurements were made in air at ambient pressure. The temperatures of the top, wall, and bottom surfaces were set to 5°, 11°, and 26°C, respectively, resulting in a vertical temperature difference of $\Delta T = 21$ K. The Rayleigh number, which represents the balance between gravitational and viscous damping forces, was on the order of 10^9 for the boundary conditions and chamber height of 1 m.

This experiment generated steady-state cloud conditions for more than 10 h. A 3-h subset of the time series is shown in Fig. 6. The top panel is the air temperature measured by those RTDs closest to the floor and the ceiling, showing that the convection is indeed stationary in time. (The sensors are both about 14 cm away from the corresponding boundary

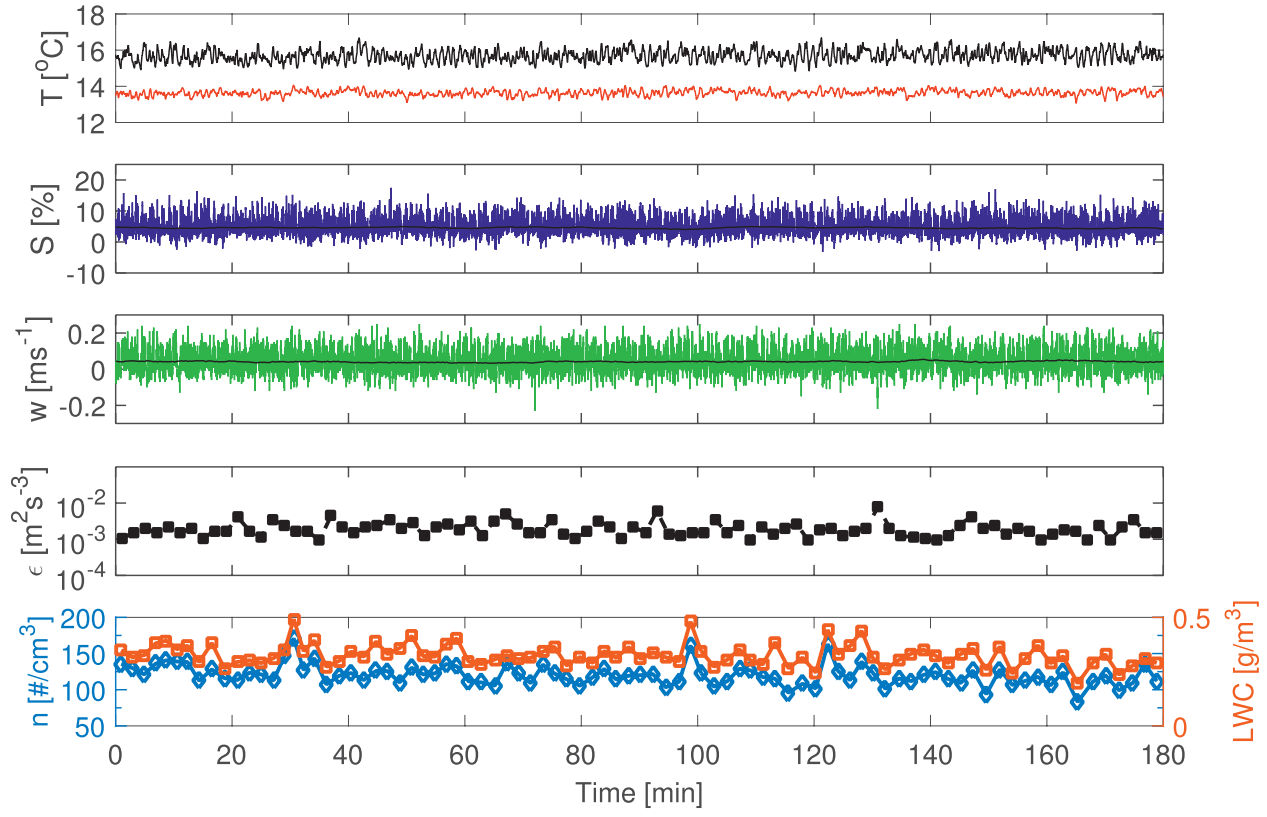

Fig. 6. Time series of temperature, supersaturation, vertical velocity, turbulent kinetic energy dissipation rate, cloud droplet number density, and liquid water content for a steady-state mixing cloud.

surface and about 38.5 cm away from the sidewalls.) Note that the mean temperature difference between the two sensors is about 2 K. The measurements suggest that there is a single major convection cell that fills the whole chamber (as in Gasteuil et al. 2007). The temperature fluctuation detected by the lower RTD is larger compared to the fluctuation measured by the upper one as the former sensor is close to the heated floor panel.

The second panel of Fig. 6 depicts the supersaturation based on the water vapor partial pressure determined from the H_2O analyzer measurements (at 20 Hz) and the saturation vapor pressure that is based on the temperature measurement closest to the H_2O analyzer. Here, it is clearly observed that fluctuations in temperature and especially in water vapor concentration lead to a randomly, strongly varying supersaturation. The mean supersaturation is approximately 5% and therefore much larger than supersaturation in atmospheric clouds, which is usually not much above 1% [e.g., for stratocumulus clouds supersaturation is in the range of 0.1% (Ditas et al. 2012)]. The third panel shows the vertical velocity component measured by the sonic anemometer at 20 Hz. From its power spectrum, averaged over a time interval of 4 min, the turbulent kinetic energy dissipation rate was calculated (panel 4) as a measure for the degree of turbulence inside the chamber. It is in the same range as observed in the cloudy boundary layer in the midlatitudes (e.g., Siebert et al. 2006). The bottom panel shows the cloud droplet number density and the liquid water content, as derived from the PDI. We note that the fluctuations here are rather large because of the limited sampling statistics over a broad size distribution, but the values are steady within that range. It is worth noting that this mode of cloud formation, allowing steady cloud microphysical conditions for times much greater than typically available in an expansion chamber, opens up a number of experimental possibilities. For example, one can envision experiments in which long time sampling is helpful, such as for studying fluctuating processes like turbulence–cloud interactions, low signal processes like some chemical reactions, or rare events like droplet collisions.

The droplet size distribution corresponding to the same steady cloud conditions is shown in Fig. 7. Under these very strong gradient conditions, for which the mean supersaturation is several percent, cloud droplets are able to grow to surprisingly large sizes.

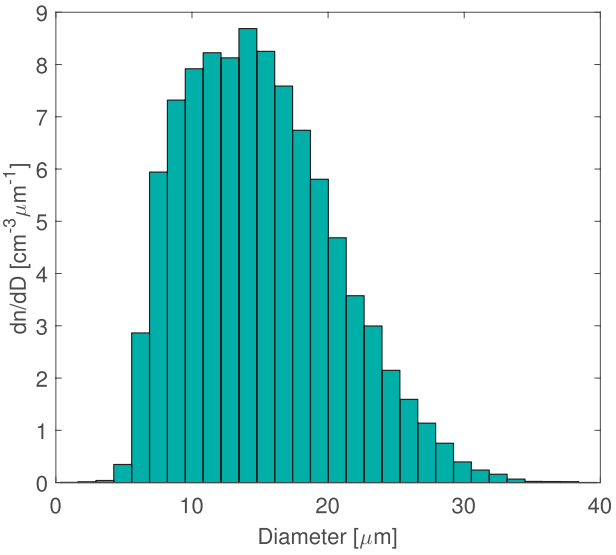

Fig. 7. Droplet size distribution for the steady mixing cloud described in Fig. 6.

The largest droplets are even approaching the drizzle range. Based on the supersaturation data and using the diffusional growth law (Rogers and Yau 1989), we estimate that droplets starting with a diameter of 1 μm could grow to about 40 μm in diameter after 1 min at a mean supersaturation of 5%. To what extent the number of CCN together with condensation in an environment with fluctuating supersaturations and collision coalescence in the turbulent environment account for the determined droplet size distribution is a matter of current investigation.

The power spectral density for vertical velocity fluctuations during steady, convective–turbulent cloud conditions is shown in Fig. 8. The inertial subrange with –5/3 scaling is clearly observed (red line with –5/3 slope shown for reference). The inertial subrange can be expected to extend to ~1 cm, whereas the decay at larger wavenumbers shown in the figure is a manifestation of instrument averaging effects.

Table 3 summarizes the flow properties of the turbulent mixing cloud. The quantities presented in this table are introduced and described in more detail in several texts, for example, Wyngaard (2010) and Davidson (2015). All properties represent averages over the 3-h time interval. The term W represents the mean vertical velocity, measured at a point midway between the wall and center and midway between the top and bottom panels. [The vertical velocity averaged over the full horizontal cross section of the chamber must be zero, as it is a closed system, but even in turbulent convection a weak but steady circulation can result in nonzero mean velocity at a single Eulerian point; e.g., Resagk et al. (2006).] The root-mean-square (rms) average of the vertical velocity fluctuations is $w' = \langle (w-W)^2 \rangle^{1/2}$. The kinematic viscosity $\nu = 1.5 \times 10^{-5}$ m^2 s^{-1} was calculated following Morvay and Gvodenac (2008). The energy dissipation rate is estimated in two ways. First, we use the relationship $\varepsilon_1 = (S_2/C)^{3/2}/r$, where $S_2 = \langle \delta w^2(z,r) \rangle$ is the second moment of the velocity increment $\delta w(z,r) = w(z+r) - w(z)$, $\langle \cdot \rangle$ is the spatial average, z is the vertical position, r is the separation distance, and $C = 2.1$ is the Kolmogorov constant. In practice, we used Taylor's hypothesis to transform from temporal space to physical space. The last assumption is weakly applicable to flows with small mean flow, which is the case in our experiment where the ratio of the velocity fluctuation to mean is approximately 1.3. Second, we obtain the integral of the dissipative spectrum $k^2 E(k)$, which for isotropic turbulence is $\int k^2 E(k)\, dk = 2\varepsilon_2/(15\nu)$.

The integral length L is estimated by integrating the correlation function $\langle w(z+r)w(z) \rangle / w'^2$. The Kolmogorov length and time scales are given by $\eta = (\nu^3/\varepsilon_2)^{1/4}$ and $\tau_\eta = (\nu/\varepsilon_2)^{1/2}$. We obtain the Taylor scale through the relation $\lambda = (15\nu\, w'^2/\varepsilon_2)$. The Taylor Reynolds number of the flow is given by $R_\lambda = w'\, \lambda/\nu$. The latter four calculations are based on the ε_2 value that was determined from the integral of the dissipative spectrum. The measurements of L and

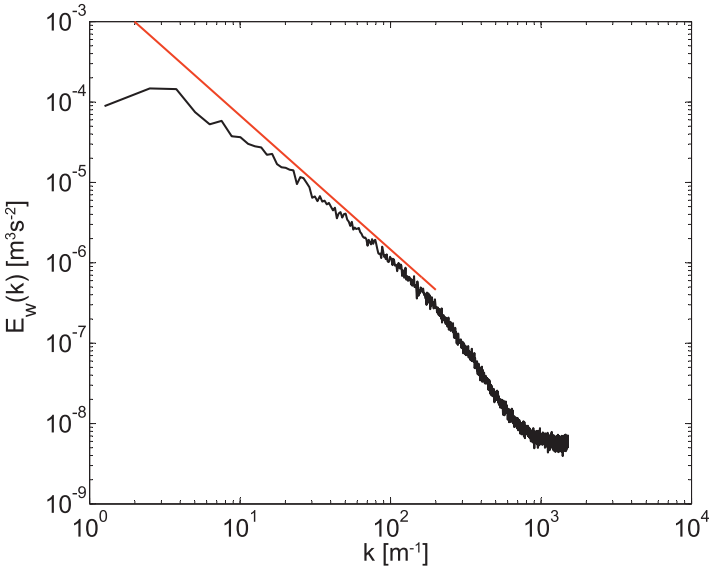

Fig. 8. Turbulent velocity power spectrum for the steady mixing cloud described in Fig. 6. A red line with –5/3 slope expected for the inertial range of the turbulent energy cascade is shown for reference.

Table 3. Turbulence parameters calculated from measurements during the steady-state turbulent mixing experiment.

Boundary condition	W (cm s^{-1})	w' (cm s^{-1})	ε_1 (m^{2}s^{-3})	ε_2 (m^{2}s^{-3})	L (cm)	η (mm)	τ_η (s)	λ (cm)	R_λ
Wet	4.2	5.4	1.1×10^{-3}	2.7×10^{-3}	8.8	1.1	0.27	1.6	55

R_λ are much smaller than the values typically encountered in atmospheric clouds. However, for studies of small-scale interactions of droplets and turbulence, this is not a limitation (Siebert et al. 2010). The Taylor Reynolds number is in the range of values determined in other Rayleigh–Bénard convection experiments (e.g., Ni et al. 2012).

RESULTS FROM PRELIMINARY EXPERIMENTS. The range of research areas that may be addressed with the Π chamber is broad. We have chosen three examples with preliminary data as a preview of the results to come. As noted in the introduction, one motivation for developing the chamber is to study the interplay between turbulence and cloud processes down to the scale of individual droplets. The results shown in the section titled "Steady-state turbulent mixing cloud" suggest several fruitful lines of inquiry. Another direction of research that will provide rich opportunities is the investigation of mixed-phase turbulent clouds. As a qualitative example, Fig. 9 shows cloud formation in steady, turbulent convection with driving (boundary) temperatures of +10° and –10°C. The cloud "plumes" are made visible by illumination with a thin sheet of laser light with images taken at a forward scatter angle of approximately 7°. Under these conditions, we are intrigued by the distinct characteristics of the warm, upward-propagating plumes and the cold, downward-propagating plumes. We selected this particular image because it shows a "collision" between two such plumes (upper-left part of the image). The warm plume has strikingly sharp boundaries, whereas the cold plume is more diffuse. A movie of the collision event is available (http://digitalcommons.mtu.edu/physics-fp/12/), and the contrast between the plume structures is even more evident there. We interpret the differing interface sharpness as a manifestation of the distinct droplet phase relaxation times. The phase relaxation time, which is the time scale for exponential relaxation of a population of droplets to the ambient thermodynamic conditions, can be approximated as $\tau_{phase} \approx (4\pi D' n \bar{r})^{-1}$, where n and $\bar{r}$ are the number density and mean radius of the cloud droplet population, and D' is a modified water vapor diffusion coefficient (Kostinski 2009; Kumar et al. 2013). The temperature dependence of D' results in increasing τ_{phase} with decreasing T, meaning cloud droplets change size more slowly at lower temperatures when responding to changes in their water vapor environment. Finding the turbulence time scale equal to τ_{phase} yields a length scale that can be considered the transition between uniform (homogeneous) mixing and nonuniform (inhomogeneous) mixing (Korolev and Mazin 2003; Lehmann et al. 2009). We speculate that the vivid contrast in cloud edge sharpness observed in Fig. 9 is a result of this difference in cloud droplet response; cold droplets are sluggish (i.e., they grow/evaporate slowly) and therefore are mixed by somewhat larger eddy sizes before responding, while relatively warm droplets are agile and respond on smaller eddy scales within the turbulent energy cascade. Quantitative investigation of this speculation is the subject of ongoing research.

A more quantitative example of aerosol–cloud interactions, this time in a warm cloud, is shown in Fig. 10. Here,

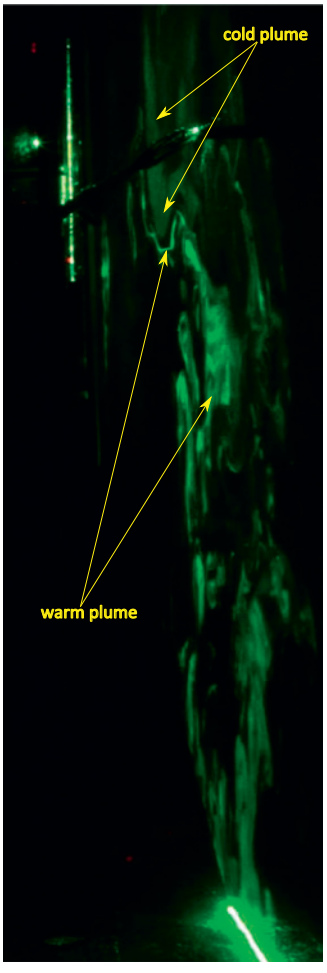

Fig. 9. A warm plume originating at the bottom surface of the chamber collides with a plume of supercooled droplets from the top surface of the chamber. The difference in "sharpness" of the plumes is readily evident. The bright vertical line at the upper left is where the laser light sheet enters the chamber through a window, and the bright diagonal line at the bottom is where the light sheet illuminates the bottom surface of the chamber.

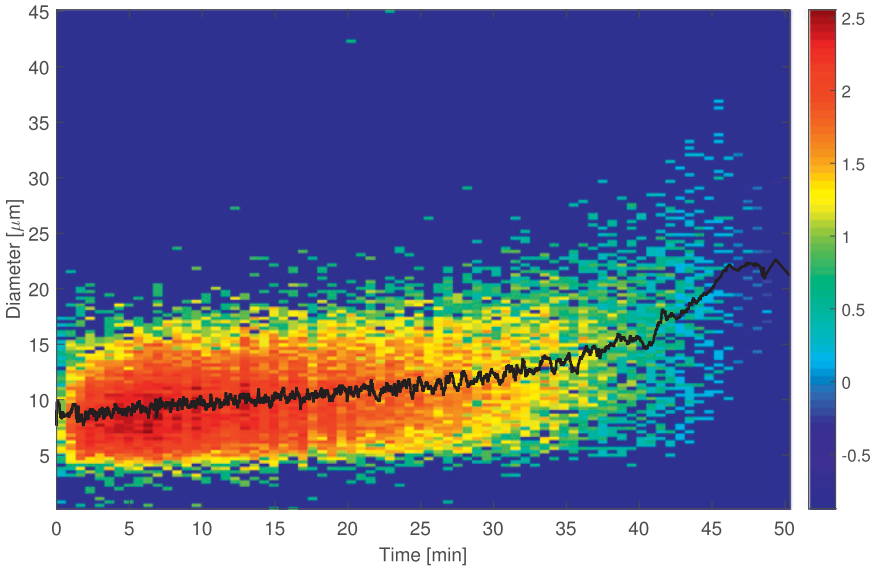

Fig. 10. Cloud droplet size distribution vs time during a transient aerosol response experiment (aerosols injected into the chamber during the first 2 min; see text for details). The color scale corresponds to the logarithm of the droplet size distribution (log10 of concentration in units of cm^{-3} mm^{-1}), and the black line is a running mean for droplet diameter.

a convective–turbulent cloud is formed when aerosols are injected for the first 2 min (between $t = 0$ and $t = 2$ min). When the aerosol source is turned off, we observe the transient response of the cloud as aerosols are removed through scavenging and through settling of cloud droplets. As the number of CCN diminishes, the cloud droplet number density decreases correspondingly, and the cloud droplet size distribution shifts to larger sizes. That shift is also observed in the running mean droplet diameter, denoted by the solid black line. This is essentially an illustration of one part of the Twomey (first indirect) effect (Twomey 1991), given that the thermodynamic driving force (i.e., the boundary conditions) is fixed, and the only change is in the number of aerosol particles. As the number density of cloud droplets becomes quite small, there is a sharp increase in the diameter, suggesting the possibility of a nonlinear response, perhaps because of the onset of collision–coalescence. The robustness of this result could be questioned because of the low counting statistics, but repeated experiments consistently show very similar, sudden increases in droplet diameter as observed in Fig. 10. The transient response of a turbulent cloud to sudden changes in aerosol conditions is intriguing and is a prime example of the kinds of idealized studies that can be carried out in a laboratory setting and then further examined and compared to field and modeling studies.

The Π chamber is also being used for studies of multiphase chemistry. As an illustrative test, the aqueous phase oxidation of S(IV) to S(VI) within suspended cloud droplets has been explored. While the formation of sulfate (SO_4^{2-}) as an experiment is not novel, this experiment helps to establish the preferred conditions and methods to perform chemical reactions in the chamber. For this purpose, we chose the reaction between dissolved sulfur dioxide (SO_2) and hydrogen peroxide (H_2O_2) as described in the literature (Seinfeld and Pandis 1998, p. 366). Cloud droplets were activated on NaCl aerosol generated from solution (0.121 g L^{-1}) using a constant output atomizer. Control experiments with NaCl aerosol and SO_2 gas were performed without H_2O_2. Oxidation experiments were conducted by adding 10 mM H_2O_2 to a separate NaCl atomizer solution (0.123 g L^{-1}). Two replicate chamber experiments of each type were performed (Table 4). Aerosol size distributions were observed using a scanning mobility particle sizer (SMPS) after a silica gel diffusion dryer and are provided in Fig. 11. Cloud droplet samples were collected using a particle into liquid sampler (PILS) with a LiBr-spiked (1.00 μM) carrier eluent as

Table 4. Results from SO_2 oxidation experiments.

Experiment type	Control 1	Control 2	Oxidation 1	Oxidation 2
PILS sample [Cl^-] (μM)	8.37	3.23	2.27	2.88
PILS sample [SO_4^{2-}] (μM)	0.00	0.422	21.40	20.00
PILS sample [Br^-] (μM)	1.04	0.880	0.798	0.828
Calculated aerosol [Cl^-] ($\mu g\ m^{-3}$)	15.80	6.10	4.30	5.44
Calculated aerosol [SO_4^{2-}] ($\mu g\ m^{-3}$)	0.00	1.94	98.40	91.90

an internal standard. Chloride (Cl^-), sulfate (SO_4^{2-}), and bromide (Br^-) concentrations in PILS samples were analyzed by ion chromatography (IC), and undiluted anion concentrations are provided in Table 4.

Concentrations of Cl^- and SO_4^{2-} in the chamber air were derived from the PILS samples (Table 4) using $[C_g] = [C_l]\, Q_{in} R/Q_a$. Here, C_g is the aerosol–gas phase concentration, C_l is the liquid sample concentration, Q_{in} is the flow rate of the carrier liquid, R is the dilution factor, and Q_a is the volumetric flow rate of air entering the PILS. The concentration of Br^- was used to determine the dilution factor R. The concentration of Cl^- in PILS samples was similar between the control and oxidation experiments, but a significantly higher concentration of SO_4^{2-} was detected in the oxidation experiments compared to the control experiments. The low concentration of SO_4^{2-} detected in the control experiments was attributed to the oxidation reaction involving oxygen catalyzed by trace quantities of transition metals, present in the atomizer solution. Figure 11 shows the change in the measured aerosol size distributions upon oxidation. Normalized number distributions from two replicate control and two replicate oxidation experiments are shown in the upper panel. The distributions are monomodal for the control, but the aerosol distributions with SO_2 oxidation have a pronounced shoulder. The reaction-produced sulfate is highlighted in the lower panel, where the corresponding normalized volume distributions are plotted. The significant increase in SO_4^{2-} concentration in PILS samples, the shift in aerosol size distribution, and the observed growth of total aerosol volume are all unambiguous evidence of the conversion of S(IV) to S(VI) by aqueous H_2O_2. These results serve as proof of concept for multiphase chemical reactions in the Π chamber, which simulates cloud processing and cloud cycles in a steady-state environment.

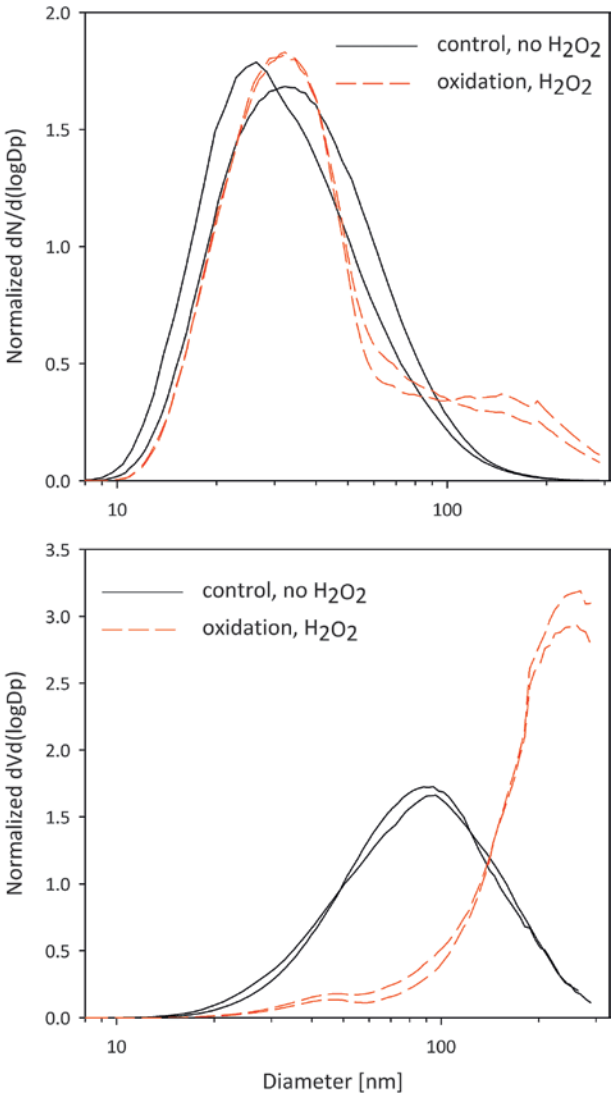

Fig. 11. Aerosol size distributions illustrating oxidation of SO_2 to sulfate. (top) Normalized number distributions from two control (without H_2O_2) and two oxidation experiments. The pronounced shoulder for larger diameters is evidence of aqueous phase conversion of SO_2 to sulfate. (bottom) Normalized volume distributions from the same experiments showing the dramatic increase in aerosol mass as a result of the aqueous phase oxidation.

SUMMARY AND OUTLOOK. We have developed a facility capable of generating cloud conditions in two ways. The first is by reducing the pressure in the chamber, thereby simulating an updraft in the atmosphere, and the second is by forcing a temperature difference between two parallel, water-coated plates, inducing moist Rayleigh–Bénard convection. The more traditional mode via expansion produces a cloud lifetime limited by how long the expansion can be maintained (on the order of 10 min). Cloud formation through mixing allows the cloud to be sustained as long as the temperature difference is maintained and cloud condensation nuclei are supplied; in practice, such cloud conditions have been maintained for many days during extended measurement studies. Operation using both modes simultaneously is also possible.

Laboratory experiments have the advantage of allowing us to decouple the full complexity of the atmosphere. Often, model comparisons with field results, as important as these are, are confounded by the lack of steady conditions, poor characterization of initial and boundary conditions, relatively sparse measurements, and the sheer level of complexity

of the many interacting processes. Cloud chamber facilities such as the one described in this paper allow focused experiments to be performed in which specific processes are isolated under well controlled and repeatable conditions. As a result, mechanisms can be identified and explored in the context of theoretical models (Hagen 1979; Ghan and Schwartz 2007). We envision that this will allow for evaluation of basic theoretical concepts underlying most models and their parameterizations, including activation and scavenging of aerosols, cloud droplet growth, and evaporation in a turbulent environment due to homogeneous and inhomogeneous mixing, ice nucleation, aqueous chemical reactions and aerosol–gas processing, and even drop growth through collision and coalescence.

We look forward to the Π chamber playing a role in understanding specific connections among clouds, aerosols, trace gases (e.g., water vapor), thermodynamics, and turbulence. We also look forward to extending our current collaborations to new issues with the cloud chemistry and physics community.

ACKNOWLEDGMENTS. The chamber development was supported by National Science Foundation Grant AGS-1039742. D. Niedermeier acknowledges support from the Alexander von Humboldt Foundation during the time this research was carried out. We thank Andrew Robare and James Spaight for their assistance with aerosol measurements.

REFERENCES

Aitken, J., 1889: Dust particles in the atmosphere at Ben Nevis Observatory. *Nature*, **40**, 350–352, doi:10.1038/040350a0.

Beard, K. V., and H. R. Pruppacher, 1969: A determination of the terminal velocity and drag of small water drops by means of a wind tunnel. *J. Atmos. Sci.*, **26**, 1066–1072, doi:10.1175/1520-0469(1969)026<1066:ADOTTV>2.0.CO;2.

Bewley, G. P., E.-W. Saw, and E. Bodenschatz, 2013: Observation of the sling effect. *New J. Phys.*, **15**, 083051, doi:10.1088/1367-2630/15/8/083051.

Bodenschatz, E., S. P. Malinowski, R. A. Shaw, and F. Stratmann, 2010: Can we understand clouds without turbulence? *Science*, **327**, 970–971, doi:10.1126/science.1185138.

Cantrell, W., and A. Heymsfield, 2005: Production of ice in tropospheric clouds: A review. *Bull. Amer. Meteor. Soc.*, **86**, 795–807, doi:10.1175/BAMS-86-6-795.

Connolly, P. J., C. Emersic, and P. R. Field, 2012: A laboratory investigation into the aggregation efficiency of small ice crystals. *Atmos. Chem. Phys.*, **12**, 2055–2076, doi:10.5194/acp-12-2055-2012.

Davidson, P. A., 2015: *Turbulence: An Introduction for Scientists and Engineers*. 2nd ed. Oxford University Press, 630 pp.

DeMott, P. J., and D. C. Rogers, 1990: Freezing nucleation rates of dilute solution droplets measured between –30° and –40°C in laboratory simulations of natural clouds. *J. Atmos. Sci.*, **47**, 1056–1064, doi:10.1175/1520-0469(1990)047<1056:FNRODS>2.0.CO;2.

Ditas, F., R. A. Shaw, H. Siebert, M. Simmel, B. Wehner, and A. Wiedensohler, 2012: Aerosols-cloud microphysics-thermodynamics-turbulence: Evaluating supersaturation in a marine stratocumulus cloud. *Atmos. Chem. Phys.*, **12**, 2459–2468, doi:10.5194/acp-12-2459-2012.

Duft, D., and T. Leisner, 2004: The index of refraction of supercooled solutions determined by the analysis of optical rainbow scattering from levitated droplets. *Int. J. Mass Spectrom.*, **233**, 61–65, doi:10.1016/j.ijms.2003.11.020.

Duplissy, J., and Coauthors, 2010: Results from the CERN pilot CLOUD experiment. *Atmos. Chem. Phys.*, **10**, 1635–1647, doi:10.5194/acp-10-1635-2010.

Feingold, G., and H. Siebert, 2009: Cloud-aerosol interactions from the micro to the cloud scale. *Clouds in the Perturbed Climate System: Their Relationship to Energy Balance, Atmospheric Dynamics, and Precipitation*, J. Heintzenberg and R. J. Charlson, Eds., MIT Press, 319–338.

Fremaux, C. M., and D. M. Bushnell, 2011: A state-of-the-art experimental laboratory for cloud and cloud-aerosol interaction research. NASA Tech. Memo. NASA/TM-2011-217192, NASA Langley Research Center, 41 pp.

Gasteuil, Y., W. Shew, M. Gibert, F. Chilla, B. Castaing, and J.-F. Pinton, 2007: Lagrangian temperature, velocity, and local heat flux measurement in Rayleigh-Bénard convection. *Phys. Rev. Lett.*, **99**, 234–302, doi:10.1103/PhysRevLett.99.234302.

Ghan, S. J., and S. E. Schwartz, 2007: Aerosol properties and processes: A path from field and laboratory measurements to global climate models. *Bull. Amer. Meteor. Soc.*, **88**, 1059–1083, doi:10.1175/BAMS-88-7-1059.

Hagen, D. E., 1979: A numerical cloud model for the support of laboratory experimentation. *J. Appl. Meteor.*, **18**, 1035–1043, doi:10.1175/1520-0450(1979)018<1035:ANCMFT>2.0.CO;2.

——, J. Schmitt, M. Trueblood, J. Carstens, D. R. White, and D. J. Alofs, 1989: Condensation coefficient measurement for water in the UMR cloud

simulation chamber. *J. Atmos. Sci.*, **46**, 803–816, doi:10.1175/1520-0469(1989)046<0803:CCMFWI>2.0.CO;2.

Hoppel, W. A., G. M. Frick, J. W. Fitzgerald, and B. J. Wattle, 1994: A cloud chamber study of the effect that nonprecipitating water clouds have on the aerosol size distribution. *Aerosol Sci. Technol.*, **20**, 1–30, doi:10.1080/02786829408959660.

Khlystou, A., G. P. A. Kos, and H. M. ten Brink, 1996: A high-flow turbulent cloud chamber. *Aerosol Sci. Technol.*, **24**, 59–68, doi:10.1080/02786829608965352.

Korolev, A. V., and I. P. Mazin, 2003: Supersaturation of water vapor in clouds. *J. Atmos. Sci.*, **60**, 2957–2974, doi:10.1175/1520-0469(2003)060<2957:SOWVIC>2.0.CO;2.

Kostinski, A. B., 2009: Simple approximations for condensational growth. *Environ. Res. Lett.*, **4**, 015005, doi:10.1088/1748-9326/4/1/015005.

Kumar, B., J. Schumacher, and R. A. Shaw, 2013: Cloud microphysical effects of turbulent mixing and entrainment. *Theor. Comput. Fluid Dyn.*, **27**, 361–376, doi:10.1007/s00162-012-0272-z.

Lamb, D., and J. Verlinde, 2011: *Physics and Chemistry of Clouds*. Cambridge University Press, 584 pp.

Latham, J., and R. L. Reed, 1977: Laboratory studies of the effects of mixing on the evolution of cloud droplet spectra. *Quart. J. Roy. Meteor. Soc.*, **103**, 297–306, doi:10.1002/qj.49710343607.

Lehmann, K., H. Siebert, and R. A. Shaw, 2009: Homogeneous and inhomogeneous mixing in cumulus clouds: Dependence on local turbulence structure. *J. Atmos. Sci.*, **66**, 3641–3659, doi:10.1175/2009JAS3012.1.

List, R., J. Hallett, J. Warner, and R. Reinking, 1986: The future of laboratory research and facilities for cloud physics and cloud chemistry. *Bull. Amer. Meteor. Soc.*, **67**, 1389–1397.

——, G. B. Lesins, F. Garcia-Garcia, and D. B. McDonald, 1987: Pressurized icing tunnel for graupel, hail and secondary raindrop production. *J. Atmos. Oceanic Technol.*, **4**, 454–463, doi:10.1175/1520-0426(1987)004<0454:PITFGH>2.0.CO;2.

Lu, J., H. Nordsiek, E. W. Saw, and R. A. Shaw, 2010: Clustering of charged inertial particles in turbulence. *Phys. Rev. Lett.*, **104**, 184505, doi:10.1103/PhysRevLett.104.184505.

Möhler, O., and Coauthors, 2003: Experimental investigation of homogeneous freezing of sulphuric acid particles in the aerosol chamber AIDA. *Atmos. Chem. Phys.*, **3**, 211–223, doi:10.5194/acp-3-211-2003.

Morvay, Z., and D. Gvodenac, 2008: *Applied Industrial Energy and Environmental Management*. John Wiley & Sons, 434 pp.

National Research Council, 2003: *Critical Issues in Weather Modification Research*. National Academies Press, 144 pp., doi:10.17226/10829.

Ni, R., S.-D. Huang, and K.-Q. Xia, 2012: Lagrangian acceleration measurements in convective thermal turbulence. *J. Fluid Mech.*, **692**, 395–419, doi:10.1017/jfm.2011.520.

Petters, M. D., and S. M. Kreidenweis, 2007: A single parameter representation of hygroscopic growth and cloud condensation nucleus activity. *Atmos. Chem. Phys.*, **7**, 1961–1971, doi:10.5194/acp-7-1961-2007.

Quaas, J., and Coauthors, 2009: Current understanding and quantification of clouds in the changing climate system and strategies for reducing critical uncertainties. *Clouds in the Perturbed Climate System: Their Relationship to Energy Balance, Atmospheric Dynamics, and Precipitation*, J. Heintzenberg and R. J. Charlson, Eds., MIT Press, 557–573, doi:10.7551/mitpress/9780262012874.003.0024.

Resagk, C., R. du Puits, A. Thess, F. V. Dolzhansky, S. Grossmann, F. F. Araujo, and D. Lohse, 2006: Oscillations of the large scale wind in turbulent thermal convection. *Phys. Fluids*, **18**, 095105, doi:10.1063/1.2353400.

Rogers, R. R., and M. K. Yau, 1989: *A Short Course in Cloud Physics*. 3rd ed. Pergamon Press, 293 pp.

Rzesanke, D., J. Nadolny, D. Duft, R. Müller, A. Kiselev, and T. Leisner, 2012: On the role of surface charges for homogeneous freezing of supercooled water microdroplets. *Phys. Chem. Chem. Phys.*, **14**, 9359–9363, doi:10.1039/c2cp23653b.

Seinfeld, J. H., and S. N. Pandis, 1998: *Atmospheric Chemistry and Physics*. Wiley, 1326 pp.

Siebert, H., K. Lehmann, and M. Wendisch, 2006: Observations of small-scale turbulence and energy dissipation rates in the cloudy boundary layer. *J. Atmos. Sci.*, **63**, 1451–1466, doi:10.1175/JAS3687.1.

——, S. Gerashchenko, A. Gylfason, K. Lehmann, L. R. Collins, R. A. Shaw, and Z. Warhaft, 2010: Towards understanding the role of turbulence on droplets in clouds: In situ and laboratory measurements. *Atmos. Res.*, **97**, 426–437, doi:10.1016/j.atmosres.2010.05.007.

Song, N., and D. Lamb, 1994: Experimental investigations of ice in supercooled clouds. Part 1: System description and growth of ice by vapor deposition. *J. Atmos. Sci.*, **51**, 91–103, doi:10.1175/1520-0469(1994)051<0091:EIOIIS>2.0.CO;2.

Stehle, R. L., A. W. Gertler, U. Katz, D. Lamb, and D. F. Miller, 1981: Cloud chamber studies of dark transformations of sulfur dioxide in cloud droplets. *Atmos. Environ.*, **15**, 2341–2352, doi:10.1016/0004-6981(81)90264-X.

Stetzer, O., B. Baschek, F. Lüönd, and U. Lohmann, 2008: The Zurich Ice Nucleation Chamber (ZINC)—A new instrument to investigate atmospheric ice formation. *Aerosol Sci. Technol.*, **42**, 64–74, doi:10.1080/02786820701787944.

Stratmann, F., and Coauthors, 2004: Laboratory studies and numerical simulations of cloud droplet formation under realistic supersaturation conditions. *J. Atmos. Oceanic Technol.*, **21**, 876–887, doi:10.1175/1520-0426(2004)021<0876:LSANSO>2.0.CO;2.

——, O. Möhler, R. Shaw, and H. Wex, 2009: Laboratory cloud simulation: Capabilities and future directions. *Clouds in the Perturbed Climate System: Their Relationship to Energy Balance, Atmospheric Dynamics, and Precipitation*, J. Heintzenberg and R. J. Charlson, Eds., MIT Press, 149–172.

Tajiri, T., K. Yamashita, M. Murakami, A. Saito, K. Kusunoki, N. Orikasa, and L. Lilie, 2013: A novel adiabatic-expansion-type cloud simulation chamber. *J. Meteor. Soc. Japan*, **91**, 687–704, doi:10.2151/jmsj.2013-509.

Twomey, S., 1991: Aerosols, clouds and radiation. *Atmos. Environ.*, **25A**, 2435–2442, doi:10.1016/0960-1686(91)90159-5.

Wallace, J. M., and P. V. Hobbs, 1977: *Atmospheric Science: An Introductory Survey*. 1st ed. Academic Press, 467 pp.

Wang, J., J. F. Doussin, S. Perrier, E. Perraudin, Y. Katrib, E. Pangui, and B. Picquet-Varrault, 2011: Design of a new multi-phase experimental simulation chamber for atmospheric photosmog, aerosol and cloud chemistry research. *Atmos. Meas. Tech.*, **4**, 2465–2494, doi:10.5194/amt-4-2465-2011.

Wilson, C. T. R., 1911: On a method of making visible the paths of ionising particles through a gas. *Proc. Roy. Soc. London*, **A85**, 285–288, doi:10.1098/rspa.1911.0041.

Wyngaard, J. C., 2010: *Turbulence in the Atmosphere*. 1st ed. Cambridge University Press, 393 pp.